Preprints, 26th Conf. on Radar Meteorology, Norman, OK, AMS, May 24-28, 1993, 417-420.

THE SECONDARY BAND AND REFLECTIVITY TROUGH IN A MIDLATITUDE SQUALL LINE: INSIGHTS FROM THERMODYNAMIC AND MICROPHYSICAL RETRIEVAL

Scott A. Braun and Robert A. Houze, Jr.

Department of Atmospheric Sciences, AK-40
University of Washington
Seattle, WA 98195 USA

1. INTRODUCTION

Convective systems characterized by a leading line of strong convective precipitation followed by a region of stratiform precipitation are a rather common mode of organization of squall lines (Houze et al. 1990). A typical feature of these systems is a *secondary maximum* of radar reflectivity within the trailing stratiform precipitation region. Often this secondary maximum takes the form of a band (the *secondary band*) of intensified stratiform precipitation parallel to the convective line. Ligda (1956) was apparently the first to document this maximum, as well as the accompanying minimum of reflectivity located between it and the leading line of convection. The zone of minimum radar reflectivity is sometimes called the *reflectivity trough* or *transition zone*. It has been examined by Smull and Houze (1985, 1987), Rutledge and Houze (1987), Biggerstaff and Houze [1991, 1993 (hereafter referred to as BH93)], and Matejka and Schuur (1992).

Several hypotheses, or contributing factors, have been suggested and examined regarding the development of the transition zone minimum and secondary maximum of the radar reflectivity in squall lines with trailing stratiform precipitation. These hypotheses fall into three general categories. Some suppose that the reflectivity trough is at least partially the result of downward air motion and evaporation in the transition zone (Ligda 1956; BH93). A second hypothesis is that the horizontal distribution of precipitation, and radar reflectivity, behind the convective line is a purely kinematic consequence of the locations at which precipitation particles originating in the cells of the leading convective line eventually fall out as a result of their terminal fallspeeds and the horizontal wind (Smull and Houze 1985; Rutledge and Houze 1987). A third hypothesis suggests that the horizontal distribution of precipitation to the rear of the convective line is not so much a result of trajectories of particles, or suppression of growth by downdrafts in the transition zone, but rather the result of upward air motion in the vicinity of the secondary maximum (Matejka and Schuur 1992).

These past studies have given evidence that all of the suggested mechanisms are feasible and probably active to some extent. The purpose of this study is to determine quantitatively which of the mechanisms were dominant in a squall line that passed over Oklahoma and Kansas on 10-11 June 1985. Since this squall line is of a rather common type, the results obtained here probably apply more generally than to this case alone.

2. RETRIEVAL METHODOLOGY

The retrieval method used for the present analysis closely follows that of Hauser et al. (1988) and Marecal et al. (1993). The microphysical fields are obtained by using the bulk microphysical parameterizations of Lin et al. (1983) and Rutledge and Hobbs (1983), and solving two-dimensional, steady-state conservation equations for the microphysical variables. Temperature and pressure are determined in a manner similar to the dynamic method of Hauser et al. (1988).

3. DATA AND RETRIEVAL RESULTS

The wind field used in the retrieval is taken from a composite of dual-Doppler-synthesized wind fields for the northern portion of the 10-11 June 1985 PRE-STORM * squall line during the mature stage of the system. The composite data set has horizontal and vertical resolution of 3 and 0.5 km, respectively (see BH93 for details). An average vertical cross section oriented normal to the squall line was obtained by averaging over a 60-km wide strip perpendicular to the line. Figure 1a shows the mean reflectivity and vectors of the two-dimensional storm-relative wind in the plane of the cross section, and Figure 1b shows the average vertical velocity. The cross section is characterized by a 60-km wide leading convective line, followed by a region of stratiform precipitation nearly 150 km wide. Within the stratiform region is the secondary band (x = –70 to 35 km). The transition zone, defined by the low-level reflectivity minimum between $x \approx 35$ and 60 km, is seen between the convective and stratiform precipitation regions.

Fig. 2a shows the mixing ratios of rain (q_r) and precipitating ice (q_p) obtained from the retrieval. In the convective region, q_r values of up to 1.5 g kg^{-1} are diagnosed, while q_p reaches about 3.6 g kg^{-1} near 8 km. Distinct minima are present in the retrieved fields of rain *and precipitating ice* between x = 15 and 30 km, and distinct secondary maxima of rain and precipitating ice are present at the horizontal position of the weak mesoscale updraft (between x = –50 and 15 km).

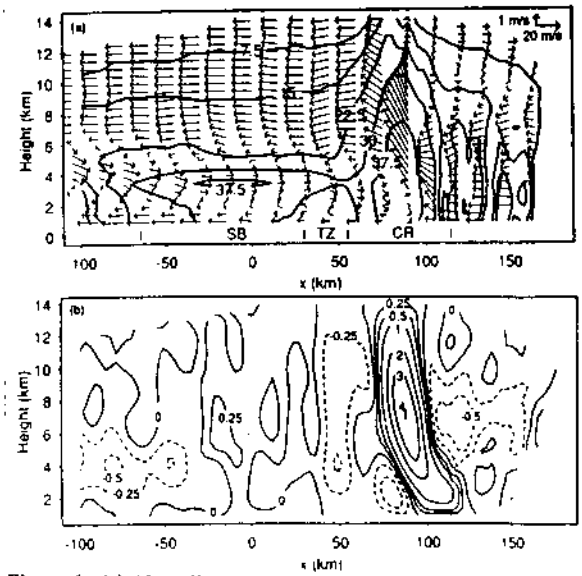

Figure 1. (a) Along-line averaged radar reflectivity and wind vectors in the plane of the cross section. The arrows in the upper right corner represent the arrow scales. The approximate positions of the secondary band (SB), transition zone (TZ), and convective region (CR) are indicated along the bottom of the figure. (b) Along-line averaged vertical velocity (m s^{-1}).

* PRE-STORM is an acronym for Oklahoma-Kansas Preliminary Regional Experiment for the Stormscale Operational and Research Meteorology Program-Central Phase.

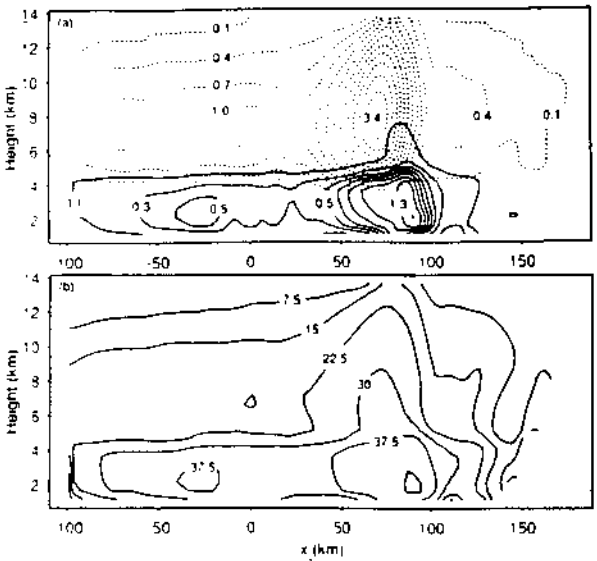

Figure 2. (a) Mixing ratios (g kg^{-1}) of rain (solid) and precipitating ice (dotted). Contours are drawn every 0.2 g kg^{-1} for rain and every 0.3 g kg^{-1} for precipitating ice, starting at 0.1 g kg^{-1}. (b) Reflectivity (dbZ) determined from the rain and precipitating ice mixing ratios.

For comparison with the observed reflectivity field in Fig. 1a, the equivalent reflectivity factor Z_e (or reflectivity, for short) is computed from the retrieved rain and precipitating ice mixing ratios following Fovell and Ogura (1988). The effects of melting ice are not included in this calculation. The retrieved reflectivity field (expressed in dBZ) is shown in Figure 2b. Comparison with Fig. 1a indicates that, aside from the difficulties in accounting for the enhancement of the reflectivity in melting layers, the reflectivity field is well reproduced. However, the secondary band and reflectivity trough are much less distinct in Fig. 2b than in the observed reflectivity field shown in Fig. 1a. These results suggest that, although the secondary band (reflectivity trough) corresponds to a secondary maximum (a relative minimum) of precipitation, the precipitation amount (Fig. 2a) alone does not account for the observed radar reflectivity pattern. As demonstrated by BH93, the radar reflectivity pattern is strongly affected by aggregation, the effects of which are not included in the retrieval.

4. THE SECONDARY BAND AND REFLECTIVITY TROUGH

In this section, we investigate the processes responsible for the formation of the secondary band maximum and transition-zone minimum in reflectivity. We group these processes into two general categories: those which change the amount of precipitation (e.g., by vapor deposition) and those which change the reflectivity but not the precipitation mass (e.g., by aggregation). Therefore, we divide this discussion into two parts. In Section 4a, we describe the processes which act to increase the precipitation mass in the secondary band. In Section 4b, we discuss the processes acting to enhance the aggregation rates over the secondary band region and the effects of aggregation on the reflectivity field.

4.1 Development of the secondary maximum and transition zone minimum of precipitation

In Fig. 3, we show particle trajectories computed using the Doppler-radar observed winds (Fig. 1) and the retrieved mass-weighted fallspeeds. The trajectories were calculated backwards from just under the melting level (3.8 km) until they reached the convective updraft. Dots are drawn every 20 min along the trajectories. The line at $x = 40$ km is used to indicate the rear edge of the convective precipitation as determined from Fig. 2a. The trajectories are overlaid on the production rates of precipitating ice associated with deposition and sublimation. Also shown are precipitating ice mixing ratios (labeled PIDEP) determined by integrating the production rates associated with deposition and sublimation along each trajectory from just below the melting level to $x = 40$ km. The integration was terminated at $x = 40$ km since our interest is in the growth which occurs after particles leave the convective region.

The highest deposition rates are observed in the convective updraft where the water vapor perturbations and precipitating ice mixing ratios are greatest. The front-to-rear (FTR) flow in the stratiform region is supersaturated with respect to ice. Most of the depositional growth in the stratiform region FTR flow occurs within the layer between 6 and 10 km, with maximum rates in the vicinity of the mesoscale updraft between $x = -30$ and 30 km. Behind the convective line, sublimation occurs below 6 km in association with the transition zone downdraft and the descending rear inflow at the back edge of the stratiform region. Above 6 km, the transition zone downdraft ($x = 50$ km) is supersaturated with respect to ice. In the presence of the descent, this supersaturation was maintained by the rearward advection of water vapor from the convective region by the FTR flow. Although the mean transition zone descent was supersaturated with respect to ice, actual individual downdrafts may have been subsaturated, producing local sublimation.

The particle trajectories in Fig. 3 are nearly identical to those presented in BH93. Upon exiting the convective region, particles following trajectory 6 reach the melting level in the retrieved transition zone and fall out quickly so that only limited growth occurs by deposition. This lesser growth is reflected in the integrated values of precipitating ice mixing ratio associated with deposition, which is minimum along trajectory 6. Trajectories 2 - 5, which span the width of the secondary band, are suspended in the deposition layer for longer times (~1 to 2 h compared to 20 min in the case of trajectory 6) and pass directly through the region of strongest mesoscale ascent. The integrated growth by deposition is highest along these trajectories. The back edge of the secondary band and the decreasing rainfall to the rear are associated with particles following trajectories 1 and 2 which, although suspended aloft for the longest times, pass above the region of strongest mesoscale ascent and strongest growth by deposition.

These results suggest that the secondary maximum in precipitation is the result of the long residence times within the mesoscale ascent of ice particles ejected from upper levels of the convective region. Since the depositional growth enhances the precipitation mass some distance rearward of the convective line, a relative minimum in precipitation is produced in the transition zone. Additional retrieval results (not shown here) indicate that the subsidence in the transition zone contributes somewhat to the precipitation minimum by suppressing particle growth. However, this descent was not the cause of the minimum.

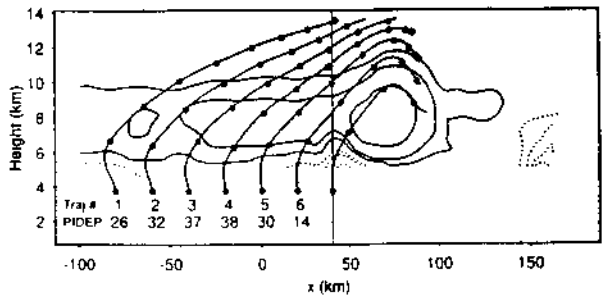

Figure 3. Particle trajectories and precipitating ice production rates. The contours are the production rates of precipitating ice associated with deposition (solid) and sublimation (dotted), drawn at values of ± 0.5, 1.0, and 2.0 x 10^{-7} kg kg^{-1} s^{-1}. Integrated mixing ratios (PIDEP, lower left) are expressed in hundredths of g kg^{-1}. See text for further explanation.

4.2 Effects of aggregation on reflectivity

BH93 used the composite reflectivity field (Fig. 1a) to determine mean reflectivity profiles for the secondary band, transition zone, and convective region (Fig. 4). The mean reflectivity in the secondary band increased approximately 16 dBZ between 6 km (–10°C) and 3.6 km (just below the 0°C level), with much of this increase occurring in a 1 km deep layer just above the melting level. Conversely, in the transition zone, the mean reflectivity increased gradually by about 9 dBZ between the same levels. Since the radar reflectivity is a strong function of particle size (proportional to D^6!), they inferred that rapid particle growth by aggregation occurred above the melting level in the secondary band region and did not occur as strongly in the transition zone.

BH93 further noted that the reflectivity above 5 km over the secondary band region was slightly less than that in the transition zone (Fig. 4). Consequently, they suggested that growth by vapor deposition did not directly produce the secondary maximum in reflectivity. Indeed, Fig. 3 shows that the depositional growth occurred above 6 km, while the rapid increase in size occurred below this level (Fig. 4). However, the retrieval does indicate slightly greater precipitating ice mass in the mesoscale updraft region (Fig. 2a), and this higher concentration of ice mass is the result of vapor deposition. The lower reflectivity at upper levels in the secondary band implies that *the greater amount of ice mass there is distributed over a higher concentration of smaller particles.* A higher concentration of smaller particles with greater total mass per unit mass of air can lead to greater aggregation within the secondary band region (Hobbs et al. 1974).

In addition to increasing the mass of precipitation in the secondary band region, the depositional growth in the mesoscale ascent also produces ice crystals which tend to aggregate. Hobbs et al. (1974) showed that the maximum size of aggregates depends on the component crystal habits, with aggregates composed of dendrites (which form between –12°C and –16°C) generally having the largest size. Houze and Churchill (1987) associated the formation of large aggregates above the melting layer in the stratiform precipitation areas of tropical mesoscale convective systems with the presence of dendrites just above the layer of aggregation. In a study of wintertime stratiform precipitation over the mountains of northwestern Colorado, Rauber (1987) found that significant aggregation did not occur unless dendritic crystals were present. Therefore, the difference in aggregation rates in the secondary band and transition zone may result from differences in particle habits, with the secondary band being characterized by large aggregates of dendritic crystals. Such aggregates, along with needles (produced between –4°C and –6°C), aggregates of needles, and other unidentifiable aggregates, were detected by aircraft in the secondary band region (Rutledge et al. 1988). To show that conditions in the secondary band region were conducive to the growth of dendritic crystals, we show in Fig. 5 the retrieved temperatures (°C) and relative humidities. The mesoscale updraft region (x = –30 to 30 km) was generally supersaturated with the supersaturation extending downward to the melting level between x = –30 and –5 km. These conditions indicate that dendritic growth was likely near the 7 km level over the approximately 60 km wide region of mesoscale ascent.

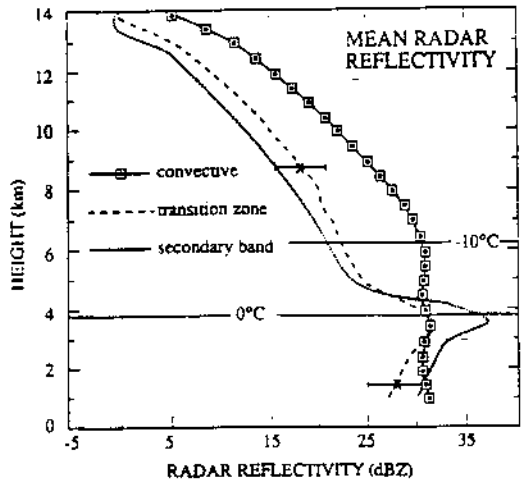

Figure 4. Mean reflectivity (dBZ) profiles (from BH93).

In the transition zone, the lower retrieved humidities prevented the growth of dendritic particles and actually produced sublimation below 6 km (Fig. 3). This result supports the hypothesis of BH93 that descent within the transition zone produced an unfavorable environment for aggregation leading to smaller particles below the melting level there.

The effects of aggregation can be included in an *ad hoc* manner by considering the impact of aggregation on the size distribution of the precipitation. The considerable aggregation occurring above the observed bright band modifies the particle size distributions such that very large raindrops and high reflectivities occur below the melting level. Since aggregation increases (decreases) the concentration of larger (smaller) particles, the slope of the assumed exponential size distribution, and the intercept parameter N_0, should tend to be lower in regions of strong aggregation and higher where aggregation is weak (Stewart et al. 1984).

In the case of the 10-11 June squall line, we suggest that a drop in N_0 occurred within the transition zone as a result of the strong aggregation in the secondary band. It is conventional to assume a constant N_0 in a bulk microphysical parameterization of the type used in the microphysical retrieval. To illustrate the effects of an N_0-drop on the retrieved reflectivity, we deviated from this convention and reran the microphysical retrieval allowing for a drop in N_0 for rain by an order of magnitude between the convective and stratiform regions, with this transition occurring at x = 25 km, roughly the middle of the transition zone rain minimum (Fig. 2a). For $x \geq 25$ km, N_0 was set to 8×10^6 m^{-4} as in the control run, while for $x < 25$ km, N_0 was set to 8×10^5 m^{-4}.

Fig. 6a shows the rain and precipitating ice mixing ratios, and Fig. 6b the retrieved reflectivity, for the N_0-drop case. The rain mixing ratios have decreased by 0.1 to 0.3 g kg^{-1} in the secondary band region. Despite the weaker secondary maximum in rain mixing ratio in the stratiform region, a distinct secondary maximum in radar reflectivity is present there. The enhancement of the reflectivity begins immediately at the N_0-drop location (x = 25 km), leaving a distinct gap in the reflectivity between the convective region and secondary band. This case demonstrates the strong dependence of the reflectivity field on aggregation, which strongly affects the particle size distribution of the rain which results from the melting of the aggregates.

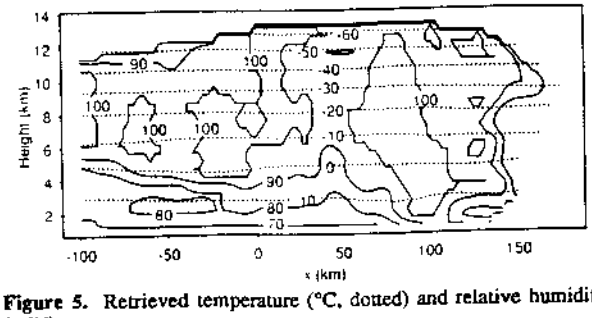

Figure 5. Retrieved temperature (°C, dotted) and relative humidity (solid).

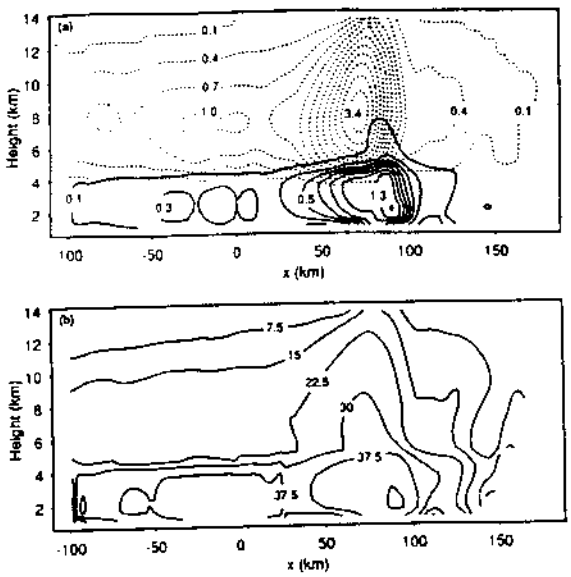

Figure 6. As in Fig. 2, but for the N_0-drop case.

5. CONCLUSIONS

Thermodynamic and microphysical retrieval techniques have been applied to dual-Doppler synthesized air motion fields for a midlatitude squall line, which passed through the PRE-STORM observational array in Kansas and Oklahoma on 10-11 June 1985. The retrieval reproduces the general precipitation structure of the squall line. The retrieved fields further indicate the processes producing the secondary maximum and transition zone minimum of radar reflectivity more quantitatively than has been possible in previous studies. The primary processes accounting for these features of the precipitation pattern were 1) the substantial growth by deposition of vapor onto precipitating ice particles generated in and detrained from convective cells and falling out through the region of mesoscale ascent in the stratiform region, 2) the strong aggregation of ice particles above the bright band in the region of the secondary band, which affected the size distribution of raindrops below the bright band such that the reflectivity was enhanced, and 3) the suppression of growth in the mid-to-upper level descent just behind the convective region, which slightly enhanced the minimum of radar reflectivity in that zone.

Acknowledgments: We would like to thank Drs. F. Roux and J. Sun for making the temperature retrieval software available to us, and Dr. M. Biggerstaff for providing us with the synthesized dual-Doppler radar data set used in this study. G. C. Gudmundson edited the manuscript. This research was sponsored by National Science Foundation grant ATM-610230.

REFERENCES

Biggerstaff, M. I., and R. A. Houze, Jr., 1991: Kinematic and precipitation structure of the 10-11 June 1985 squall line. *Mon. Wea. Rev.*, **119**, 3034-3065.

Biggerstaff, M. I., and R. A. Houze, Jr., 1993: Kinematics and microphysics of the transition zone of a midlatitude squall-line system. *J. Atmos. Sci.*, (conditionally accepted).

Fovell, R. G., and Y. Ogura, 1988: Numerical simulation of a midlatitude squall line in two dimensions. *J. Atmos. Sci.*, **45**, 3846-3879.

Hauser, D., F. Roux, and P. Amayenc, 1988: Comparison of two methods for the retrieval of thermodynamic and microphysical variables from Doppler-radar measurements: Application to the case of a tropical squall line. *J. Atmos. Sci.*, **45**, 1285-1303.

Hobbs, P. V., S. Chang, and J. D. Locatelli, 1974: The dimensions and aggregation of ice crystals in natural clouds. *J. Geophys. Res.*, **79**, 2199-2206.

Houze, R. A. Jr., and D. D. Churchill, 1987: Mesoscale organization and cloud microphysics in a Bay of Bengal depression. *J. Atmos. Sci.*, **44**, 1845-1867.

Houze, R. A. Jr., B. F. Smull, and P. Dodge, 1990: Mesoscale organization of springtime rainstorms in Oklahoma. *Mon. Wea. Rev.*, **118**, 613-654.

Ligda, M. G. H., 1956: The radar observations of mature prefrontal squall lines in the midwestern United States. *VI Congress of Organisation Scientifique et Technique Internationale du Vol a Voile (OSTIV)*, Aeronautical International Federation, St-Yan, France, 1-3.

Lin, Y.-L., R. D. Farley, and H. D. Orville, 1983: Bulk parameterization of the snow field in a cloud model. *J. Clim. Appl. Meteor.*, **22**, 1065-1092.

Marecal, V., D. Hauser, and F. Roux, 1993: The 12-13 January 1988 narrow cold-frontal rainband observed during MFDP / FRONTS 87. Part II: Microphysics. *J. Atmos. Sci.*, (in press).

Matejka, T., and T. J. Schuur, 1992: The relationship between vertical air motions and the precipitation band in the stratiform region of a squall line. Preprints, *25th Conference on Radar Meteorology*, Boston, Amer. Meteor. Soc., 501-504.

Rauber, R. M., 1987: Characteristics of cloud ice and precipitaion during wintertime storms over the mountains of northern Colorado. *J. Clim. Appl. Meteor.*, **26**, 488-524.

Rutledge, S. A., and P. V. Hobbs, 1983: The mesoscale and microscale structure and organization of clouds and precipitation in midlatitude cyclones. VIII: A model for the "seeder-feeder" process in warm frontal rainbands. *J. Atmos. Sci.*, **40**, 1185-1206.

Rutledge, S. A., and R. A. Houze, Jr., 1987: A diagnostic modeling study of the trailing stratiform region of a midlatitude squall line. *J. Atmos. Sci.*, **44**, 2640-2656.

Rutledge, S. A., R. A. Houze, Jr., A. J. Heymsfield, and M. I. Biggerstaff, 1988: Dual-Doppler and airborne microphysical observations in the stratiform region of the 10-11 June MCS over Kansas during PRE-STORM. Preprints, *Tenth Int. Cloud Physics Conf.* Ofenbach am Main: Deutscher Wetterdienst, 705-707.

Smull, B. F., and R. A. Houze, Jr., 1985: A midlatitude squall line with a trailing region of stratiform rain: Radar and satellite observations. *Mon. Wea. Rev.*, **113**, 117-133.

Smull, B. F., and R. A. Houze, Jr., 1987: Dual-Doppler radar analysis of a midlatitude squall line with a trailing region of stratiform rain. *J. Atmos. Sci.*, **44**, 2128-2148.

Stewart, R. E., J. D. Marwitz, J. C. Pace, and R. E. Carbone, 1984: Characteristics through the melting layer of stratiform clouds. *J. Atmos. Sci.*, 41, 3227-3237.